

A New Spectral Class of Brown Dwarfs at the Bottom of the IMF in IC 348

K. L. LUHMAN^{1,2} AND C. ALVES DE OLIVEIRA³

¹*Department of Astronomy and Astrophysics, The Pennsylvania State University, University Park, PA 16802, USA; kll207@psu.edu*

²*Center for Exoplanets and Habitable Worlds, The Pennsylvania State University, University Park, PA 16802, USA*

³*European Space Agency, European Space Astronomy Centre, Camino Bajo del Castillo s/n, 28692 Villanueva de la Cañada, Madrid, Spain*

ABSTRACT

In a previous study, we used JWST to identify three new brown dwarfs in the center of a nearby star-forming cluster, IC 348. The faintest object had an estimated mass of 3–4 M_{Jup} , making it a contender for the least massive brown dwarf confirmed with spectroscopy. Two of the new brown dwarfs also exhibited absorption features from an unidentified aliphatic hydrocarbon, which were not predicted by atmospheric models and were not previously detected in atmospheres outside of the solar system. We have used JWST to perform a deeper survey for brown dwarfs across a larger field in IC 348. We have identified 39 brown dwarf candidates in NIRC*am* images and have obtained spectra for 15 of them with NIRS*pec*, nine of which are classified as substellar members of the cluster. The faintest new members have mass estimates of $\sim 2 M_{\text{Jup}}$, providing a new constraint on the minimum mass of the IMF. Two new members (~ 2 and $10 M_{\text{Jup}}$) exhibit large excess emission from circumstellar disks, demonstrating that they harbor the raw materials for planet formation. Finally, eight of the nine new brown dwarfs and one known member that is newly observed with NIRS*pec* show the aforementioned hydrocarbon features. Among the total of 11 brown dwarfs in IC 348 that have hydrocarbon detections, the features are stronger at fainter magnitudes, indicating that the hydrocarbon is a natural constituent of the atmospheres of the coolest newborn brown dwarfs. We propose a new spectral class “H” that is defined by the presence of the 3.4 μm fundamental band of the hydrocarbon.

1. INTRODUCTION

The first known brown dwarfs were identified through a search for companions to nearby stars (Nakajima et al. 1995; Oppenheimer et al. 1995) and a survey for free-floating members of the Pleiades open cluster (Stauffer et al. 1994; Rebolo et al. 1995, 1996; Basri et al. 1996). Soon after those discoveries, spectroscopy in nearby star-forming regions revealed members that were cool enough to be substellar according to evolutionary models (Hillenbrand 1997; Luhman et al. 1997). Those regions offered the opportunity to detect brown dwarfs at particularly low masses since substellar objects are expected to have higher luminosities at younger ages. The young cluster IC 348 is one of the best sites for a survey for newborn brown dwarfs because it is nearby (~ 300 pc), rich (~ 500 members), and only moderately obscured by dust from its molecular cloud ($A_V < 4$, Lada & Lada 1995; Herbig 1998; Herbst 2008). Over the last three decades, we have used optical and infrared (IR) imaging and spectroscopy to pursue a thorough survey for the members of IC 348 down to the lowest possible masses (Luhman et al. 1998; Luhman 1999; Luhman et al. 2003, 2005b; Muench et al. 2007; Alves de Oliveira et al. 2013; Luhman et al. 2016; Esplin & Luhman 2017; Luhman & Hapich 2020; Luhman et al. 2024), uncovering 71 probable brown

dwarfs ($> M_6$). Two additional substellar members were found by Allers & Liu (2020).

The James Webb Space Telescope (JWST, Gardner et al. 2023) is capable of detecting members of nearby star-forming regions down to masses of $\sim 1 M_{\text{Jup}}$. IC 348 is one of the few nearby young clusters that is sufficiently compact ($D \sim 0.5^\circ$) for imaging with JWST, which has a small field of view. During Cycle 1 of the mission, we used NIRC*am* (Rieke et al. 2005, 2023) to obtain images of a 6.0×4.2 field in the center of the cluster (Luhman et al. 2024, hereafter L24). We identified brown dwarf candidates in those data and performed spectroscopy with the Near-Infrared Spectrograph (NIRS*pec*, Jakobsen et al. 2022) that confirmed three of them as young late-type objects, one of which is a strong contender for the least massive free-floating brown dwarf that has a spectral classification (3–4 M_{Jup}). In addition, two of the new brown dwarfs exhibited absorption bands from an unidentified aliphatic hydrocarbon, which were not predicted by atmospheric models and were not previously detected in atmospheres outside of the solar system. In this Letter, we seek to test scenarios for the origin of that hydrocarbon and to better constrain the substellar mass function and its minimum mass by using JWST to conduct a deeper survey for brown dwarfs across a larger field in IC 348.

2. IMAGING

2.1. NIRC*am* Observations

NIRC*am* on JWST simultaneously images nearly identical areas of sky through short and long wavelength channels (0.7–2.4 and 2.4–5 μm). The short/long wavelength (SW/LW) channels contain eight/two 2040×2040 detector arrays with pixel sizes of $0''.031/0''.063$. The detectors cover two $2'2 \times 2'2$ fields that are separated by $43''$. The set of detectors in each of the two fields is described as a module. In each module, the four detectors for the short wavelength channel are separated by $5''$.

We obtained NIRC*am* images of a $16' \times 20'$ field in IC 348 through program 4866 in August and September of 2024, which was during Cycle 3 of JWST’s science operations. The observations were performed with the FULLBOX dither pattern, four dithers, and a mosaic pattern containing nine rows and three columns. Each of the 27 cells in the mosaic was observed in a separate visit. In Figure 1, we have plotted a map of the members of IC 348 that were identified prior to this study (Section 1). We have marked the boundaries of the fields observed by NIRC*am* in Cycle 1 (L24) and Cycle 3 (this work). A given position in the new mosaic was covered by 2–4 exposures per filter. Each exposure utilized five groups, one integration, and the SHALLOW4 readout pattern, corresponding to an exposure time of 258 s. We selected the minimum complement of filters (two in each channel) for distinguishing brown dwarfs from other astronomical sources, which consisted of F162M, F182M, F360M, and F444W. The charged time was 41.4 hrs.

2.2. NIRC*am* Data Reduction

To reduce the NIRC*am* data, we began by retrieving the `uncal` files from the Mikulski Archive for Space Telescopes (MAST): [doi:10.17909/0hke-p124](https://doi.org/10.17909/0hke-p124). We processed the data with version 1.16.1 of the JWST Science Calibration pipeline under context `jwst_1296.pmap`. We applied detector-level corrections to the `uncal` files using the `calwebb_detector1` pipeline module. The resulting count rate images (`rate`) were processed with the `calwebb_image2` module, producing calibrated unrectified exposures (`cal`).

Registration of NIRC*am* images is performed with the `tweakreg` routine within the `calwebb_image3` module. Source-finding algorithms like those within `tweakreg` often produce spurious detections in areas of extended emission and in the point spread functions of bright stars, both of which are prevalent in a star-forming cluster like IC 348. Therefore, we initially combined the images for a given band into a mosaic with `tweakreg` deactivated, which assumed that the default world coordinate systems (WCSs) of the images were correct. We used the `starfind` routine in IRAF to identify sources in each mosaic, and we rejected those that appeared in only one band. The mosaics were visually inspected to remove remaining spurious detections. The result-

ing catalog of reliable detections served as the basis of sources used by `tweakreg` when registering images.

NIRC*am* images can be registered to an external catalog of sources that have high precision astrometry, or they can be registered internally using sources that appear in overlapping images. High precision astrometry is available from the third data release of the Gaia mission (Gaia Collaboration et al. 2016, 2021, 2023), but the mosaic in IC 348 encompasses only ~ 100 non-saturated Gaia sources, so most of the individual NIRC*am* images contain few Gaia sources, if any. Therefore, internal registration of the images was the only option.

When `tweakreg` is applied simultaneously to all of the NIRC*am* detectors for a given filter, it solves for a single offset for all of the detectors, which means that the relative WCSs for the detectors are assumed to be accurate. However, noticeable errors are present in the relative WCSs for some bands (Luhman 2024). Ideally, one would avoid such errors by measuring a separate offset for each detector during registration, but there is too little overlap among the dithered images, even for the larger detectors in the LW channel. The best approach for internal registration is to assume that the relative WCSs of the two arrays in a LW band are accurate (i.e., measure a single offset for both arrays), in which case there is enough overlap among dithered pairs of LW detectors for internal registration across the entire mosaic. We selected the F360M band for this stage of the registration.

We applied `tweakreg` to all `cal` files in F360M, solving for offsets in both x/y positions and rotation among overlapping images and solving for global offsets in position and rotation for the entire mosaic relative to Gaia DR3. We calculated the average rotation offset for the four dithers in a given visit. Since those dithered images should have identical orientations, we used `tweakreg` to rotate the `cal` files in a visit by that average offset. We processed those rotated images with `tweakreg`, solving only for the x/y offsets. The registered frames in F360M were combined into a mosaic using the `calwebb_image3` module.

For `cal` files in F162M, F182M, and F444W, we used `tweakreg` to apply the same rotation offsets that were derived for F360M. For a given visit and module in F444W, we applied `tweakreg` to the rotated frames at the four dither positions, solving for relative x/y offsets and a global x/y offset relative to the source catalog for the final F360M mosaic. The dithered images for a given detector in the SW bands do not overlap, so each of those images was aligned individually to the F360M catalog. The registered images were then combined with `calwebb_image3`. A color composite of the mosaic images for three of the four filters is presented in Figure 2.

We identified sources in the four mosaic images and measured aperture photometry for them in the manner described by Luhman (2024). Photometry was mea-

sured for aperture radii of 2, 2.5, and 4 pixels. The band-merged catalog contains ~ 9400 sources.

2.3. Identification of Brown Dwarf Candidates

Many of the sources in the NIRC*am* images of IC 348 are galaxies. As done in L24, we have used the differences in photometry between aperture radii of 2 and 4 pixels to identify sources that are likely to be resolved galaxies. In Figure 3, we have plotted m_{162} versus the median difference of the 2 and 4 pixel photometry from among the bands in which a given source is detected. We classify sources below and above a value of 0.1 as point-like and extended, respectively.

In Figure 4, we present color-color and color-magnitude diagrams in which brown dwarfs can be distinguished from most other astronomical sources, consisting of $m_{162} - m_{444}$, $m_{162} - m_{182}$, and m_{162} versus $m_{360} - m_{444}$. We have plotted all point sources from the NIRC*am* images that have nonsaturated detections in all four bands, and we have marked the previously known members. We have selected thresholds in each diagram that capture the known members with $m_{360} - m_{444} > 0.2$ and that should be sufficiently relaxed to account for reddening, IR excesses, and the undetermined trend of magnitude versus color for undiscovered members down to the bottom of the mass function. The known members with $m_{360} - m_{444} < 0.2$, which are missed by our selection criteria, have spectral types earlier than L0. The previous census of IC 348 has a high level of completeness at those spectral types (Luhman et al. 2016, hereafter L16).

We have identified the point sources that satisfy all of the thresholds in Figure 4. A star that is blended with other objects can appear to be extended based on the metric in Figure 3, so we have identified sources that are flagged as extended and that satisfy our photometric selection criteria, and we have inspected their images to check if they are blended point sources. In addition, we have inspected the images of all candidates selected from Figure 4 to verify that they are point sources and check for close companions or contamination from bad pixels. One of the candidates (LRL 11044) does have a possible secondary companion at a separation of $0''.23$ (LRL 11043). We also inspected the images of previously known members that are not saturated, resulting in the identification of a candidate companion at a separation of $0''.27$ from LRL 1546 (L0). The two pairs are well-resolved in the SW images and are partially blended in the LW images, as shown in Figure 5. In each of the LW bands, we fit and subtracted the point spread function of a given component to more accurately measure photometry for its companion. Using the resulting photometry, all components of the two pairs satisfy our selection criteria for brown dwarfs.

Our final sample of brown dwarf candidates contains 39 sources. In Figure 4, we have marked those candidates with symbols that are based on their spectral

classifications from NIRSpec (Section 3) or the absence of NIRSpec data. In Table 1, we present astrometry and photometry for the 39 candidates and the 43 previously known members that have a nonsaturated detection in at least one band.

2.4. Proper Motions

Since two epochs of NIRC*am* images are available for the center of IC 348, we can use those data to measure proper motions, which provide constraints on cluster membership. We have reprocessed the images from Cycle 1 with procedures similar to those applied to the Cycle 3 data in Section 2.2. For the Cycle 1 images in F360M, we used the catalog of galaxies from the F360M mosaic in Cycle 3 for the absolute calibration of the astrometry, which enables the measurement of absolute proper motions. The pair of dithered images for a given module was aligned to the Cycle 3 mosaic using 30–60 galaxies. We then aligned the other Cycle 1 bands to the F360M mosaic in Cycle 1 using both stars and galaxies. In Figure 6, we have plotted the proper motions measured for point sources from the two epochs of NIRC*am* data. Based on kinematic models of the Milky Way (Robin et al. 2003), most field stars in the direction of IC 348 and in the magnitude range of the NIRC*am* data should have proper motions of $1\text{--}5 \text{ mas yr}^{-1}$, which is consistent with the measurements in Figure 6. We have marked the six previously adopted members of the cluster that appear in both epochs and that are not saturated, which consist of LRL 595, LRL 596, LRL 621, and the three objects found in L24 (LRL 11001, LRL 11003, LRL 11004). In addition, we have indicated in Figure 6 the median proper motion from Gaia DR3 for the 40 stars in IC 348 that have the most accurate parallaxes, which corresponds to $(\mu_\alpha, \mu_\delta = 4.52, -6.23) \text{ mas yr}^{-1}$. The standard deviation of each component is $\sim 0.6 \text{ mas yr}^{-1}$. The six previous members have proper motions that are tightly grouped near the Gaia measurement for IC 348, which supports their membership in the cluster. The median NIRC*am* motion for the six members is $(\mu_\alpha, \mu_\delta = 4.1, -6.9) \text{ mas yr}^{-1}$ and the standard deviation in each component is $\sim 0.9 \text{ mas yr}^{-1}$. None of our new brown dwarf candidates from Cycle 3 appear within the field imaged in Cycle 1.

3. SPECTROSCOPY

3.1. NIRSpec Observations

We observed a subset of the brown dwarf candidates from Section 2.3 using the multi-object spectroscopy mode of NIRSpec on JWST (Ferruit et al. 2022) through program 4866 in February of 2025. That mode employs the microshutter assembly (MSA), which consists of four quadrants that each contain 365×171 shutters. An individual shutter has a size of $0''.2 \times 0''.46$. The MSA covers a field with a size of $3''.6 \times 3''.4$. Spectra are collected with two 2048×2048 detector arrays that

have pixel sizes of $0''.103 \times 0''.105$. We selected the PRISM disperser for our observations because of its sensitivity and wide wavelength coverage (0.6–5.3 μm). The spectral resolution for PRISM data ranges from ~ 40 to 300 from shorter to longer wavelengths.

The NIRSpec observations were divided among four visits, each of which was assigned an aperture position angle by the observatory. We manually searched for pointings in which the detector arrays would encompass large numbers of candidates for the four position angles. For each of those fields, we used the MSA Planning Tool (MPT) in the Astronomer’s Proposal Tool (APT) to search a small area ($\sim 20'' \times 20''$) for a pointing that would optimize the sample of observable targets, giving higher priority to fainter candidates. In addition to the brown dwarf candidates, we included “filler” targets at low priority, which consisted of known late-type members of IC 348, candidates for highly reddened background stars, and sources with $m_{360} - m_{444} > 0.45$ that did not satisfy the criteria for brown dwarf candidates (Figure 4).

When designing the MSA configurations with MPT, we required that targets would be observed at three nod positions in three adjacent shutters, which are equivalent to a single $0''.2 \times 1''.5$ slitlet. For one of the selected pointings, LRL 22705 (a known member) was observable in only two shutters while the third shutter was stuck closed, so it was not automatically selected as a target by MPT. We manually opened the two operable shutters for that object. As mentioned in Section 2.3, two of the brown dwarf candidates (LRL 11043 and LRL 11044), form a close pair ($0''.23$), and another candidate (LRL 11056) has a separation of $0''.27$ from a known substellar member (LRL 1546). The components of the $0''.23$ pair were observed in one of our four MSA configurations, aligned along the slitlet and straddling the bar between adjacent shutters. We manually opened an extra shutter so that each component would appear in an open shutter for all three nod positions. The primary for the $0''.27$ pair, LRL 1546, was one of our filler targets. The position angle of its secondary placed it outside of the slitlet during that observation.

We obtained usable spectra for 15 brown dwarf candidates and eight filler targets. Those sources are listed in Table 2. One additional target, LRL 11026, was contaminated by light from a nearby bright star, so we were unable to measure a reliable spectrum.

For each of the four MSA configurations, we collected one exposure at each of the three nod positions. For two configurations, a single exposure utilized 100 groups, one integration, and the NRSIRS2RAPID readout pattern. To avoid saturation for the brightest targets in the remaining two configurations, we used 68/45 groups and two/three integrations, both with the NRSRAPID readout pattern. The total exposure time for each configuration was ~ 4400 s. The charged time was 10.3 hrs.

3.2. NIRSpec Data Reduction

The data reduction for NIRSpec began with the retrieval of the `uncal` files from MAST: [doi:10.17909/xxg7-hc43](https://doi.org/10.17909/xxg7-hc43). As done in L24, we performed two separate reductions of the data that used the JWST Science Calibration pipeline and a custom version of the pipeline developed by the ESA NIRSpec Science Operations Team (Alves de Oliveira et al. 2018; Ferruit et al. 2022). In L24, we preferred the reduced spectra from the latter pipeline. However, we find that the latest version of the JWST Science Calibration pipeline (1.17.1) produces spectra that are comparable to those from the ESA NIRSpec pipeline. We have adopted the results from the JWST Science Calibration pipeline. The reduced spectra are presented in Figures 7–9. We have used the same pipeline to reprocess the NIRSpec data for the three brown dwarfs found in L24. Those updated reductions are included in Figure 7. All spectra have been flux calibrated using the photometry from NIRCcam.

3.3. Spectral Classifications

3.3.1. Nonmembers

Four candidates are T dwarfs based on the presence of absorption bands from methane (Figure 8). The fundamental band of CO at 4.4–5.2 μm is much weaker in the youngest L dwarfs than in old L dwarfs in the field (Luhman et al. 2023), so the strong CO bands in the T dwarfs observed by NIRSpec suggest that they are field dwarfs rather than members of IC 348. We have measured spectral types for the T dwarfs through comparison to standard spectra at 1–2.5 μm for a range of reddenings (Burgasser et al. 2006). One of the objects, LRL 11046, is not matched well by any reddened standard spectrum, but its absorption bands are suggestive of mid-T types. That object is both the reddest in $m_{360} - m_{444}$ and bluest in $m_{162} - m_{444}$ among the four T dwarfs in the NIRSpec sample. We estimated distances of 500–800 pc for the T dwarfs based on their photometry and the typical absolute magnitudes for T dwarfs at their spectral types (Dupuy et al. 2012). The four candidates for reddened background stars that were selected as filler targets do show red spectral slopes and deep ice features that indicate high extinctions (Figure 8). They are not protostars since they lack IR excesses in photometry from NIRCcam and the Spitzer Space Telescope (Lada et al. 2006; Muench et al. 2007). Two brown dwarf candidates and one filler target are active galaxies based on their redshifted emission lines (Figure 9).

3.3.2. New Members

The nine remaining brown dwarf candidates observed by NIRSpec have late spectral types based on their H_2O absorption bands. The triangular H -band continua and weak CO bands in these candidates indicate that they

are young (Lucas et al. 2001; Luhman et al. 2023), and therefore are likely members of IC 348. As a reminder, the three brown dwarfs found in L24 were classified as young members based on the same age diagnostics, and our measurements of their proper motions have further established their membership (Section 2.4). The NIRSpec data for two candidates (LRL 2296, LRL 11040) contain large excess emission at $>3.5 \mu\text{m}$ from circumstellar disks, providing additional evidence of youth.

The spectral types of the new members are discussed in Section 4. Table 2 contains the membership status and spectral classification for each NIRSpec target. It also includes redshifts measured from the galaxy emission lines (Donald Schneider, private communication).

3.4. Candidates that Lack Spectroscopy

The NIRSpec observations provide some indication of the viability of the remaining brown dwarf candidates that lack spectroscopy. Seven of the original candidates have negative colors in $m_{162} - m_{182}$ that are indicative of T dwarfs. Since four of them were found to be background T dwarfs with NIRSpec, it seems likely that the same is true for the other three candidates (LRL 11063, LRL 11066, LRL 11071). LRL 11026 and LRL 11055 resemble the galaxies in the NIRSpec sample in their colors, and the former may be slightly extended. The remaining candidates more closely match the confirmed members, although a few are somewhat redder in $m_{162} - m_{182}$, which could reflect higher reddenings. Two of the viable candidates that lack spectra (LRL 11064, LRL 11072) are fainter than the confirmed members.

4. A NEW SPECTRAL CLASS

4.1. Origin of the $3.4 \mu\text{m}$ Feature

In L24, we found two new members of IC 348 (LRL 11001, LRL 11003) that exhibited a strong absorption band near $3.4\text{--}3.5 \mu\text{m}$, which coincides with the so-called $3.4 \mu\text{m}$ feature that has been observed in the diffuse interstellar medium (ISM) (Soifer et al. 1976), meteorites and solar system dust (Wdowiak et al. 1988; Matraji et al. 2005), and the atmospheres of Saturn and Titan (Belluci et al. 2009). That feature has been attributed to fundamental stretching modes in an unidentified aliphatic hydrocarbon¹ (Sandford et al. 1991; Pendleton et al. 1994; Pendleton & Allamandola 2002). In L24, we removed the steam absorption bands of the hydrocarbon-bearing objects through division by the spectrum of a normal young L dwarf, which revealed the overtone and combination bands from the hydrocarbon at near-IR wavelengths. We concluded in L24 that the hydrocarbon resides in the atmospheres of the brown dwarfs rather than a foreground medium for the following reasons: (1) the extinctions of the brown dwarfs are

much too low for $3.4 \mu\text{m}$ absorption from the diffuse ISM; (2) the $3.4 \mu\text{m}$ feature has not been previously detected in molecular clouds, protostellar envelopes, or edge-on disks; and (3) the detections of the overtone and combination bands indicate that that hydrocarbon resides in atmospheres rather than a foreground medium.

Since model atmospheres for brown dwarfs do not predict the presence of a non-methane hydrocarbon, we speculated in L24 about possible scenarios for its origin, such as UV-induced photochemistry. With our new NIRSpec observations, there are now a total of 11 members of IC 348 that show significant detections of the $3.4 \mu\text{m}$ feature (Section 4.2, Figure 7). One additional source, LRL 11004, may also have a marginal detection. Among these objects, the strength of the feature is correlated with apparent magnitude, as illustrated in Figure 10. As discussed in Section 4.2, the NIRSpec data in IC 348 exhibit a continuum of spectral variations from (1) normal young L dwarfs to (2) weak $3.4 \mu\text{m}$ absorption in otherwise normal L-type spectra to (3) moderate $3.4 \mu\text{m}$ absorption and changes in the near-IR slopes and band strengths to (4) strong $3.4 \mu\text{m}$ absorption and a reversion to L-type near-IR slopes and band strengths. The correlation between the $3.4 \mu\text{m}$ band and apparent magnitude and the presence of a clear spectral sequence between L dwarfs and objects with that feature indicate that the hydrocarbon is a natural constituent of the coolest brown dwarfs in star-forming regions.

4.2. A Spectral Sequence for Hydrocarbon-bearing Objects

In Figure 7, we have presented the NIRSpec spectra of members of IC 348 from L24 and this work in order of the strength of the $3.4 \mu\text{m}$ feature. The first four objects lack that feature, and have the spectra of normal young L dwarfs. We have indicated in Figure 7 the spectral types produced by a comparison to young standard spectra at $1\text{--}2.5 \mu\text{m}$ (Luhman et al. 2017). Because of a degeneracy between spectral type and reddening for young L dwarfs, the reddest object, LRL 11004, can be matched by a wide range of standards (e.g., reddened L0, unreddened L5). Although the resolution of the NIRSpec data is very low at optical wavelengths, TiO and VO bands appear to be detected at $0.7\text{--}0.8 \mu\text{m}$ in the first two objects near L0, while they seem to be absent for the next two L dwarfs that are slightly later, which is consistent with previous optical spectra of young L dwarfs (Cruz et al. 2009).

The 11 objects in Figure 7 that have detections of the $3.4 \mu\text{m}$ band exhibit the following broad trends (with a few exceptions): (1) when the $3.4 \mu\text{m}$ feature first appears (LRL 40013), TiO and VO may begin to reemerge while the H₂O bands and near-IR spectral slope remain unchanged relative to normal L dwarfs; (2) as the $3.4 \mu\text{m}$ absorption increases, TiO and VO continue to strengthen, the H₂O bands weaken, and the near-IR slopes become bluer; (3) when the $3.4 \mu\text{m}$ band is

¹ We refer to the carrier in the singular, but multiple species may be responsible for the $3.4 \mu\text{m}$ feature.

strongest, the H₂O bands return to the depths of L dwarfs and the near-IR slopes may become somewhat redder. A comparison of the spectral slopes should account for the possibility of reddening (i.e., the intrinsic spectra may be bluer than the observed spectra). Regardless of reddening, it is clear that sources with intermediate 3.4 μm strengths tend to have the bluest near-IR slopes. The reversal in spectral features for those objects is reminiscent of a less extreme reversal in near-IR colors and FeH strengths across the L/T transition among field dwarfs (Burgasser et al. 2002b).

The expectation has been that the youngest brown dwarfs would show methane absorption below some temperature threshold, assuming that the initial mass function (IMF) extends to low enough masses. Instead, a different aliphatic hydrocarbon appears in the coolest newborn brown dwarfs. The challenge is for theoretical models (e.g., Zhang et al. 2025) to explain the presence of that hydrocarbon, the absence of methane, and the other spectral trends that we have observed.

4.3. The Proposed “H” Spectral Class

From earlier to later types, the beginnings of the L/T/Y spectral classes are defined primarily by the significant weakening of TiO at red optical wavelengths (L) and the onset of methane (T) and ammonia (Y) at near-IR wavelengths (Martín et al. 1997; Kirkpatrick et al. 1999; Burgasser et al. 2002a; Geballe et al. 2002; Kirkpatrick 2005; Cushing et al. 2011). Since we have identified a new population of young brown dwarfs that do not fall within any of these spectral classes, we propose the definition of a new class that is based solely on the presence of the 3.4 μm band. When considering letters to select for new classes, Kirkpatrick et al. (1999) suggested that H, L, T, and Y were the best options at that time. We propose to adopt H for the new class that is tied to the 3.4 μm feature. The letters used for spectral types often do not carry meaning, but “H” could stand for “hydrocarbon” (a non-methane aliphatic variety). We refrain from attempting to define subclasses and identify specific objects to serve as standards until a larger sample of these hydrocarbon-bearing objects is available. Depending on the trends among spectral features that emerge in a larger sample, it may be possible to define H subclasses through a combination of the 3.4 μm band and features from other species like TiO, VO, and H₂O.

5. PROPERTIES OF THE SUBSTELLAR POPULATION

5.1. Initial Mass Function

5.1.1. IMF Sample

We wish to incorporate the results of our survey for brown dwarfs in IC 348 into a new estimate of the cluster’s IMF. We have combined the compilation of members from L16 with additional mem-

bers found in subsequent studies (Esplin & Luhman 2017; Luhman & Hapich 2020; Allers & Liu 2020; Lalchand et al. 2022, L24) and in this work. We have omitted LRL 322, LRL 390, and WBIS 03441864+3218204, which we have classified as non-members based on astrometry from Gaia DR3. Only sources with spectral classifications are considered, which excludes some close companions and a few protostars. For a population like IC 348 that is associated with a molecular cloud, the members have a range of extinctions. Since more massive members can be detected through greater extinction, a sample that includes all known members is susceptible to a bias against members at lower masses. To obtain a sample of members that is unbiased in mass and that is an accurate reflection of the IMF in the cluster, it is necessary to define an extinction-limited sample in which the extinction limit is high enough to encompass a large number of members but low enough that the completeness limit reaches low masses. In L16, we found that our census of IC 348 within a large area that extended beyond the NIRCcam field had a high level of completeness down to masses of $\sim 0.01 M_{\odot}$ for extinctions of $A_J < 1.5$ ($A_K < 0.57$). Therefore, we include in our IMF sample the known members that have $A_J < 1.5$ and that are located within the NIRCcam field. The resulting sample contains 281 objects. We assume that all of the new members found with JWST in L24 and this work are within the extinction limit for the IMF sample (Section 5.1.2).

5.1.2. Histograms of Absolute Magnitudes

To characterize the IMF in terms of observational parameters that should be correlated with mass, we have plotted two histograms of extinction-corrected absolute magnitudes in Figure 11 for two pairs of similar filters. We have adopted a distance of 313 pc for all members (L24). Extinctions are taken from L16 when available in that study and otherwise are derived in the same manner. We normally estimate extinctions from a comparison of an observed spectrum or color to the typical intrinsic color or spectrum for a young photosphere with the spectral type in question, but those typical properties are undetermined for objects with the 3.4 μm feature. Therefore, we adopt $A_K = 0.2 \pm 0.2$ for those sources, which spans the extinctions for most cluster members. In one histogram in Figure 11, we have used photometry in the *H* band for the previously known members and photometry in F162M for the new members from L24 and this work. We have measured a median color of $H - m_{162} = 0.15$ for the nonsaturated members in the NIRCcam images, which we have used to convert m_{162} to *H*. For the second histogram, we have plotted photometry in F444W when available and otherwise have used data in the 4.5 μm band from Spitzer. We find no systematic offset between these bands for the known members. Some members have disk emission in those bands, which will move them to brighter

magnitude bins relative to their photospheric emission. In Figure 11, we have included histograms for the 19 viable NIRCcam candidates that lack spectroscopy (Section 3.4).

One notable feature of each histogram that combines the IMF sample and the remaining NIRCcam candidates is a bump near $M_{H/162}=10-11$ and $M_{4.5/444}=8-9$. This bump includes the objects that exhibit weak-to-moderate $3.4 \mu\text{m}$ absorption and may be equivalent to the J -band bump that has been observed at the L/T transition among field dwarfs (Dahn et al. 2002; Tinney et al. 2003; Vrba et al. 2004; Dupuy et al. 2012). Across that transition, the near-IR colors of field dwarfs become bluer, which maintains a roughly constant J -band magnitude. Similarly, the near-IR spectra of the objects in IC 348 become bluer with the onset of the $3.4 \mu\text{m}$ feature, as discussed in Section 3.3. Unlike with field dwarfs, the bump in IC 348 also appears in a band at longer wavelengths, F444W.

5.1.3. Luminosity and Mass Estimates

In Luhman (2025), we estimated an IMF for IC 348 based on the census of members prior to this study. For our new IMF sample, we adopt the same mass estimates, which were derived from (1) positions in the Hertzsprung-Russell diagram and evolutionary models ($<K0$, Luhman et al. 2003), (2) spectral types and a fit to dynamical mass as a function of spectral type for young stars ($K0-M7$), and (3) M_K and evolutionary models (Baraffe et al. 2015; Chabrier et al. 2023, $>M7$). For the new members found in L24 and this work, we have derived masses from estimates of bolometric luminosities in conjunction with evolutionary models. As done in L24, we have estimated luminosities by flux calibrating the NIRSspec data ($0.6-5.3 \mu\text{m}$) with the NIRCcam photometry, extrapolating to shorter and longer wavelengths with model spectra (Tremblin et al. 2015, 2017; Petrus et al. 2023), integrating the resulting spectra, and assuming a distance of 313 pc. This was done for both no extinction and an extinction correction of $A_K = 0.4$, where the latter was implemented with the extinction law from Schlafly et al. (2016). For the two sources with large IR excesses in their spectra, LRL 2296 and LRL 11040, we estimated their photospheric fluxes at $3.5-5 \mu\text{m}$ using other NIRSspec targets with similar $1-3 \mu\text{m}$ spectra. The luminosity estimates are included in Table 2. We have derived masses by combining those luminosities with the values predicted by Chabrier et al. (2023) for an age of 5 Myr (L24). The faintest new members have mass estimates of $\sim 2 M_{\text{Jup}}$. The evolutionary models also imply temperatures of ~ 900 K for those objects. For the viable candidates that lack spectroscopy, we have estimated luminosities from m_{444} using the correlation between that band and luminosity among the new members, and we have converted those luminosities to masses using the evolutionary models. The two faintest candidates have mass estimates of $\sim 1 M_{\text{Jup}}$. We

note that mass estimates produced by evolutionary models for young brown dwarfs below $\sim 0.05 M_{\odot}$ lack observational tests from dynamical masses, so they could have significant systematic errors. Nevertheless, even very large errors in the masses ($\sim 50\%$) would not qualitatively affect our results (i.e., the detection of objects with masses of a few M_{Jup}).

5.1.4. Characteristics of Substellar IMF

In Figure 12, we present the IMF for our extinction-limited sample of members of IC 348 in the NIRCcam field, which extends from $5 M_{\odot}$ to $2 M_{\text{Jup}}$. We have included a second histogram in which the candidates lacking spectroscopy have been added. The mass functions are plotted with logarithmic mass bins, which results in a Salpeter slope of 1.35. The statistical errors are from Gehrels (1986). The members of IC 348 with mass estimates near $\sim 2 M_{\text{Jup}}$ are the least massive known brown dwarfs that have spectral classifications, providing a significant improvement in the constraint on the minimum mass of the IMF relative to the object at $3-4 M_{\text{Jup}}$ found in L24. The two faintest candidates that lack spectroscopy suggest that the IMF could extend to even lower masses.

The substellar IMF in Figure 12 exhibits a dip in the bin centered at $\log(\text{mass}) = -2.3$ ($5 M_{\text{Jup}}$). When the photometric candidates are included, a modest peak also appears in the next higher mass bin, which coincides with the bump in the histograms of absolute magnitudes in Figure 11 and the objects with weak-to-moderate $3.4 \mu\text{m}$ bands. This structure in the mass function may reflect errors in the mass estimates that originate in the atmospheric and/or evolutionary models. Errors of this kind may not be surprising given that the models do not predict the various spectral changes that occur after the onset of the $3.4 \mu\text{m}$ feature. If we average across the bins at $\log(\text{mass}) = -2.1$ and -2.3 and include the photometric candidates, the data in Figure 12 would be consistent with a mass function that declines very slowly down to $\log(\text{mass}) = -2.5$ ($3 M_{\text{Jup}}$), and drops somewhat faster at lower masses. The constraints on the bottom of the IMF in IC 348 would be improved by spectroscopy of the remaining NIRCcam candidates and successful modeling of the hydrocarbon-bearing objects. The number ratio of stars to brown dwarfs in the IMF sample is 227/54. If all of the 19 viable candidates lacking spectra are members, the ratio would become 227/73.

5.1.5. Comparison to Other Young Clusters

In addition to IC 348, the Perseus cloud contains a second relatively rich cluster, NGC 1333, which has ~ 200 known members and is younger and more heavily obscured than IC 348. Langeveld et al. (2024) have used JWST to perform slitless spectroscopy down to $K \sim 20.5$ in an area of NGC 1333 that encompasses ~ 50 known members, identifying six brown dwarf candidates with $K = 16.4-19.2$ and mass estimates of $5-$

15 M_{Jup} . That study concluded that it had detected the least massive brown dwarfs within the survey field (i.e., the minimum mass of the IMF). However, the much deeper observations of IC 348 have uncovered members down to masses of $\sim 2 M_{\text{Jup}}$ and two candidates near the mass of Jupiter. It seems likely that a deeper survey of NGC 1333 would detect members at comparable masses.

NGC 2024 is a heavily embedded cluster in the Orion-B molecular cloud (Meyer et al. 2008; Robberto et al. 2024) that has been the target of a survey for brown dwarfs with JWST. De Furio et al. (2025) obtained very deep NIRCcam images for a single pointing in the center of the cluster, covering two neighboring fields with sizes of $2'2 \times 2'2$ (the two modules of NIRCcam). That study reported a photometric sensitivity to unreddened members with masses of $0.5 M_{\text{Jup}}$ and the detection of 48 candidates with mass estimates as low as $3 M_{\text{Jup}}$, leading them to conclude that they had measured the minimum mass of the IMF. However, none of the candidates had the spectroscopy needed for confirmation of the low temperatures and youth. In addition, coordinates and photometry were not provided for the brown dwarf candidates, so it is not possible for any later study to assess their validity (with photometry or spectroscopy) or reproduce the mass function from that study. In the Appendix, we perform an independent analysis of those NIRCcam images to identify brown dwarf candidates.

5.2. Circumstellar Disks

Two of the new members of IC 348, LRL 2296 and LRL 11040, are significantly redder at $>3.5 \mu\text{m}$ in the NIRSpc data than other cluster members at similar magnitudes, indicating the presence of excess emission from circumstellar disks. Both objects also exhibit absorption features that may arise from circumstellar ices (H_2O , CO_2 , OCN^- , CO). The IR excesses are apparent in Figure 4, where the two brown dwarfs have the reddest colors in $m_{162} - m_{444}$ and $m_{360} - m_{444}$ among the known members. Given our mass estimates of ~ 2 and $10 M_{\text{Jup}}$, the fainter one is the least massive known brown dwarf that has evidence of a disk. Two of the NIRCcam candidates that lack spectra, LRL 11052 and LRL 11059, also have similar colors that are suggestive of IR excesses. Circumstellar disks often do not produce noticeable excess emission within the wavelength range of the NIRSpc and NIRCcam data, so these disk detections provide only a lower limit for the fraction of low-mass brown dwarfs in IC 348 that harbor disks. A thorough census of disks among these objects would require observations at longer IR wavelengths. Data at longer wavelengths are available in IC 348 from the Spitzer Space Telescope (Lada et al. 2006; Muench et al. 2007), but they are not sufficiently sensitive to detect members with masses of $\lesssim 10 M_{\text{Jup}}$.

Seo & Scholz (2025) recently used a set of archival Spitzer images at 3.6 and $4.5 \mu\text{m}$ to search for IR ex-

cesses among the previously known members of IC 348 that are M9 or later. Those images had a total exposure time of 7.5 min for a given position and filter, which was described as “ultradeep”. All of the objects in question had been previously checked for IR excesses, most of them using deeper images from Spitzer that had total exposure times of 26 min (Luhman et al. 2005a; Lada et al. 2006; Muench et al. 2007). Most of the Spitzer disk classifications from Seo & Scholz (2025) and the earlier studies are in agreement. We note the few classifications that differ, and we utilize the deeper data from NIRCcam to reassess the presence of IR excesses near $4.5 \mu\text{m}$. An excess was detected for LRL 5231 by Seo & Scholz (2025) but not L16. In the NIRCcam images, this object has $m_{360} - m_{444} = 0.29$. Among other members near its spectral type (M9–L0), the bluest sources, which likely have photospheric colors, have $m_{360} - m_{444} \sim 0.15$. Thus, LRL 5231 could have a small color excess from a disk. Meanwhile, the disk classifications for LRL 6005 and LRL 30057 also differed between L16 and Seo & Scholz (2025). We measure $m_{360} - m_{444} = 0.34$ for both objects. Since both sources have uncertain spectral types (M9–L3) and the photospheric colors in $m_{360} - m_{444}$ become rapidly redder between types of late M and L (Figure 4), it is unclear whether they have color excesses.

We note that two of the previously known brown dwarfs in IC 348, LRL 1843 and LRL 30003, appear as point sources that are surrounded by extended scattered light in the NIRCcam images. Both objects are located near the protostars in the southwest corner of the cluster.

5.3. Multiplicity

Among the candidate and previously known brown dwarfs in IC 348 that are not saturated, NIRCcam has resolved two close pairs that are likely to be binary systems (Figure 5). The Hubble Space Telescope has imaged some of the saturated brown dwarfs at higher masses, none of which were resolved as binaries (Luhman et al. 2005c). A low fraction of wide binary brown dwarfs in IC 348 is consistent with previous multiplicity surveys in other star-forming regions and the solar neighborhood (Burgasser et al. 2007; Todorov et al. 2014; Opitz et al. 2016; Fontanive et al. 2023).

The new binary systems found with NIRCcam have angular separations of $0'23$ and $0'27$, which correspond to 72 and 85 AU, respectively, at the distance of IC 348. Our mass estimates are $\sim 6/12 M_{\text{Jup}}$ for LRL 11043/LRL 11044 and $\sim 8/18 M_{\text{Jup}}$ for LRL 11056/LRL 1546. These systems are rare examples of young binary brown dwarfs that have separations of >10 AU and secondary masses of $<10 M_{\text{Jup}}$. Two other binaries of this kind are 2MASSW J1207334–393254 in the TW Hya association (Chauvin et al. 2004) and 2MASS J04414489+2301513 in the Taurus star-forming region (Todorov et al. 2010).

6. CONCLUSIONS

During Cycle 1 of JWST, we obtained images of a $6'.0 \times 4'.2$ field in the center of IC 348 with NIRCcam and we performed spectroscopy on the resulting brown dwarf candidates with NIRSpec (L24). Three candidates were confirmed to be substellar members of the cluster (3–8 M_{Jup}). Two of the new members exhibited strong absorption in the $3.4 \mu\text{m}$ fundamental band and the near-IR overtone and combination bands of an unidentified aliphatic hydrocarbon, which were not predicted by atmospheric models and were not previously detected in atmospheres outside of the solar system. In Cycle 3, we have performed a deeper survey for brown dwarfs across a larger field in IC 348 ($16' \times 20'$) to test scenarios for the origin of that hydrocarbon and to better constrain the substellar mass function and its minimum mass. Our results are summarized as follows:

1. We have identified 39 brown dwarf candidates in IC 348 using color-color and color-magnitude diagrams constructed from NIRCcam photometry in F162M, F182M, F360M, and F444W. The candidates extend down to $m_{162} \sim 24$, which should correspond to masses of $\sim 1 M_{\text{Jup}}$ according to evolutionary models.
2. The new NIRCcam images have provided a second epoch of astrometry for the $6'.0 \times 4'.2$ field that was observed in Cycle 1, enabling the measurement of proper motions. The six nonsaturated sources in the Cycle 1 field that we previously adopted as members (including the three new brown dwarfs found in L24) have proper motions that are tightly clustered near the Gaia motion for IC 348, which serves as additional evidence of their membership.
3. We have used NIRSpec to obtain low-resolution 1–5 μm spectra for 15 brown dwarf candidates and eight filler targets, where the latter included three known members. Based on our analysis of the spectra, the candidates consist of nine new members of IC 348, four field T dwarfs that are in the background of the cluster (500–800 pc), and two active galaxies.
4. The new NIRSpec observations have detected the $3.4 \mu\text{m}$ hydrocarbon feature in eight of the nine new members and one previously known member. A total of 11 members of IC 348 now have detections of it. Among these objects, the strength of the feature is correlated with apparent magnitude, which indicates that the hydrocarbon is a natural constituent of the coolest brown dwarfs in star-forming regions.
5. The 11 objects that have detections of the $3.4 \mu\text{m}$ band exhibit the following trends: (1) when the $3.4 \mu\text{m}$ feature first appears, TiO and VO may begin to reemerge while the H_2O bands and near-IR spectral slope remain unchanged relative to normal L dwarfs; (2) as the $3.4 \mu\text{m}$ absorption increases, TiO and VO continue to strengthen, the H_2O bands weaken, and the near-IR slopes become bluer; (3) when the $3.4 \mu\text{m}$ band is strongest, the H_2O bands return to the depths of L dwarfs and the near-IR slopes may also return somewhat to redder slopes. Some aspects of these trends are reminiscent of the L/T transition among field dwarfs.
6. Because of the strengths of the hydrocarbon features and the other large spectral changes that accompany their onset, we propose the definition of a new spectral class (“H” for “hydrocarbon”) that is based on the presence of the $3.4 \mu\text{m}$ feature.
7. We have used the NIRSpec data to estimate bolometric luminosities for the new members of IC 348. Those luminosities have been converted to masses using evolutionary models (Chabrier et al. 2023). With mass estimates of $\sim 2 M_{\text{Jup}}$, the faintest new members are the least massive known brown dwarfs, providing an improved constraint on the minimum mass of the IMF.
8. Based on the results of our NIRSpec observations, five of the 24 remaining NIRCcam candidates that lack spectroscopy are likely to be background T dwarfs or galaxies while 19 candidates have colors that are similar to the confirmed members. Two of the latter candidates could have masses near the mass of Jupiter if they are members.
9. We have estimated the IMF for an extinction-limited sample of known members of IC 348 that are located within the NIRCcam field. The IMF is constructed with logarithmic mass bins, which results in a Salpeter slope of 1.35. Compared to previous samples of young stars used for IMF measurements, the sample in IC 348 has a unique combination of relatively large size (281 objects), spectral classifications for all members, high level of completeness for the selected range of extinctions, and a mass range that spans from $5 M_{\odot}$ to $\sim 2 M_{\text{Jup}}$. The substellar IMF for our sample exhibits structure that coincides with objects that have weak-to-moderate $3.4 \mu\text{m}$ absorption, which may reflect errors in the mass estimates that originate in the atmospheric and evolutionary models. If we ignore that structure and include the viable photometric candidates, the substellar IMF appears to decline very slowly down to $3 M_{\text{Jup}}$, and drop somewhat faster at lower masses.
10. The NIRSpec data for two new members contain large excess emission at $>3.5 \mu\text{m}$ from circumstel-

lar disks. One of these objects has a mass estimate of $\sim 2 M_{\text{Jup}}$, making it the least massive known brown dwarf with evidence of a disk.

11. Two of the new brown dwarfs have a separation of $0''.23$ (72 AU), and thus are likely to be a binary system. In addition, one of the candidates that lacks spectroscopy has a separation of $0''.27$ (85 AU) from a previously known brown dwarf. Our mass estimates are $\sim 6/12 M_{\text{Jup}}$ for the first pair and $\sim 8/18 M_{\text{Jup}}$ for the second pair. These systems are rare examples of young binary brown dwarfs that have wide separations (>10 AU) and secondary masses below $10 M_{\text{Jup}}$.

We thank Donald Schneider for measuring the redshifts of the galaxies in the NIRSpec sample. This work is based on observations made with the NASA/ESA/CSA James Webb Space Telescope. The data were obtained from MAST at the Space Telescope Science Institute, which is operated by the Association of Universities for Research in Astronomy, Inc., under NASA contract NAS 5-03127. The JWST observations are associated with program 4866. Support for program 4866 was provided by NASA through a grant from the Space Telescope Science Institute. This work made use of ESA Datalabs (<https://datalabs.esa.int>), which is an initiative by ESA's Data Science and Archives Division in the Science and Operations Department, Directorate of Science. This work used data from the ESA mission Gaia (<https://www.cosmos.esa.int/gaia>), processed by the Gaia Data Processing and Analysis Consortium (DPAC, <https://www.cosmos.esa.int/web/gaia/dpac/consortium>). Funding for the DPAC has been provided by national institutions, in particular the institutions participating in the Gaia Multilateral Agreement. The Center for Exoplanets and Habitable Worlds is supported by the Pennsylvania State University, the Eberly College of Science, and the Pennsylvania Space Grant Consortium.

APPENDIX

A. IDENTIFICATION OF BROWN DWARF CANDIDATES IN NGC 2024

De Furio et al. (2025) used NIRCcam on JWST to obtain very deep images in the center of NGC 2024 through program 1190 (PI: M. Meyer) on 2023 March 1 (UT). The observations were performed at a single pointing using subpixel dithers. Images were taken with eight filters that consisted of F070W, F115W, F140M, F182M, F356W, F360M, F430M, and F444W. The total exposure time in each filter was 2 hr.

We retrieved the `unCAL` files for program 1190 from MAST: [doi:10.17909/6t3v-px45](https://doi.org/10.17909/6t3v-px45). Those data were reduced with the JWST Science Calibration pipeline. We identified sources in the reduced images and measured aperture photometry for them with the methods applied to our data in IC 348 (Section 2.2).

Two of the filters in the data set for NGC 2024, F140M and F182M, coincide with molecular absorption bands in brown dwarfs. The combination of those bands and a filter that measures adjacent continuum, such as F162M, can produce a color-color diagram in which brown dwarfs have distinctive colors relative to most other astronomical

sources, even in the presence of reddening (e.g., Luhman 2024). Unfortunately, F162M was not included in program 1190, which reduces the utility of F140M and F182M. Given the available filters, the one color-color diagram that is useful for the identification of brown dwarf candidates is $m_{182} - m_{444}$ versus $m_{360} - m_{444}$, which is similar to a diagram that was applied to IC 348 in Figure 4. That diagram is shown in Figure 13 for the point sources in NGC 2024. We also have included a color-magnitude diagram consisting of m_{444} versus $m_{360} - m_{444}$. To help guide the selection of brown dwarf candidates, we have marked the members of IC 348 that have spectral types of $\geq L0$ and the young L dwarf TWA 27B (Luhman et al. 2023). Members of IC 348 and NGC 2024 are not perfectly comparable in a color-magnitude diagram since they have different distances and ages, but the differences in distances, age, and extinction roughly cancel each other in terms of apparent magnitudes (i.e., NGC 2024 is younger than IC 348, but it has a larger distance and higher extinctions).

In Figure 13, we have marked a reddening vector that captures TWA 27B and all of the $\geq L0$ members of IC 348. Two of the objects satisfying that threshold are sufficiently underluminous in the color-magnitude diagram relative to the members of IC 348 that we have rejected them. The remaining eight sources below the reddening vector are adopted as candidates for $\geq L0$ members of NGC 2024. The astrometry and photometry for those candidates are presented in Table 3. Two candidates have similar colors as the IC 348 sources while the remaining candidates have redder colors that suggest higher extinctions. Sources 2 and 7 appear to have the faintest extinction-corrected magnitudes, and hence are candidates for brown dwarfs with particularly low masses. According to APT, program 5409 has obtained NIRSpc spectra for sources selected from the NIRCcam images of NGC 2024. It appears that four of the eight candidates that we have identified are absent from those observations, including source 7. Because of the high extinction in NGC 2024, some sources in the images at F360M and F444W lack detections in bands at shorter wavelengths like F182M. At high reddenings, we are unable to reliably distinguish brown dwarfs from background stars and galaxies using only the former pair of bands.

REFERENCES

- Allers, K. N., & Liu, M. C. 2020, *PASP*, 132, 104401
- Alves de Oliveira, C., Birkmann, S. M., Böker, T., et al. 2018, *SPIE*, 10704, 107040Q
- Alves de Oliveira, C., Moraux, E., Bouvier, J., et al. 2013, *A&A*, 549, A123
- Baraffe, I., Horneier, D., Allard, F., & Chabrier, G. 2015, *A&A*, 577, 42
- Basri, G., Marcy, G. W., & Graham, J. R. 1996, *ApJ*, 458, 600
- Bellucci, A., Sicardy, B., Drossart, P., et al. 2009, *Icarus*, 201, 198
- Burgasser, A. J., Geballe, T. R., Leggett, S. K., Kirkpatrick, J. D., & Golimowski, D. A. 2006, *ApJ*, 637, 1067
- Burgasser, A. J., Kirkpatrick, J. D., Brown, M. E., et al. 2002a, *ApJ*, 564, 421
- Burgasser, A. J., Marley, M. S., Ackerman, A. S., et al. 2002b, *ApJL*, 571, L151
- Burgasser, A. J., Reid, I. N., Siegler, N., et al. 2007, in *Protostars and Planets V*, ed. V. B. Reipurth, D. Jewitt, & K. Keil (Tucson, AZ: Univ. Arizona Press), 427
- Chabrier, G., Baraffe, I., Phillips, M., & Debras, F. 2023, *A&A*, 671, A119
- Chauvin, G., Lagrange, A.-M., Dumas, C., et al. 2004, *A&A*, 425, L29
- Cruz, K. L., Kirkpatrick, J. D., & Burgasser, A. J. 2009, *AJ*, 137, 3345
- Cushing, M. C., Kirkpatrick, J. D., Gelino, C. R., et al. 2011, *ApJ*, 743, 50
- Dahn, C. C., Harris, H. C., Vrba, F. J., et al. 2002, *AJ*, 124, 1170
- De Furio, M., Meyer, M. R., Green, T., et al. 2025, *ApJL*, 981, L34
- Dupuy, T. J., & Liu, M. C. 2012, *ApJS*, 201, 19
- Esplin, T. L., & Luhman, K. L. 2017, *AJ*, 154, 134
- Ferruit, P., Jakobsen, P., Giardino, G., et al. 2022, *A&A*, 661, A81
- Fontanive, C., Bedin, L. R., De Furio, M., et al. 2023, *MNRAS*, 526, 1783
- Gaia Collaboration, Brown, A. G. A., Vallenari, A., et al. 2021, *A&A*, 649, A1
- Gaia Collaboration, Prusti, T., de Bruijne, J. H. J., et al. 2016, *A&A*, 595, A1
- Gaia Collaboration, Vallenari, A., Brown, A. G. A., et al. 2023, *A&A*, 674, A1
- Gardner, J. P., Mather, J. C., Abbott, R., et al. 2023, *PASP*, 135, 068001
- Geballe, T. R., Knapp, G. R., Leggett, S. K., et al. 2002, *ApJ*, 564, 466
- Gehrels, N. 1986, *AJ*, 303, 336
- Herbig, G. H. 1998, *ApJ*, 497, 736
- Herbst, W. 2008, in *Handbook of Star Forming Regions*, Vol. 1, ed. B. Reipurth (San Francisco, CA: ASP), 372
- Hillenbrand, L. A. 1997, *AJ*, 113, 1733

- Jakobsen, P., Ferruit, P., Alves de Oliveira, C., et al. 2022, *A&A*, 661, A80
- Kirkpatrick, J. D. 2005, *ARA&A*, 43, 195
- Kirkpatrick, J. D., Reid, I. N., Liebert, J., et al. 1999, *ApJ*, 519, 802
- Lada, E. A., & Lada, C. J. 1995, *AJ*, 109, 1682
- Lada, C. J., Muench, A. A., Luhman, K. L., et al. 2006, *AJ*, 131, 1574
- Lalchand, B., Chen, W.-P., Biller, B. A., et al. 2022, *AJ*, 164, 125
- Langeveld, A. B., Scholz, A., Mużić, K., et al. 2024, *AJ*, 168, 179
- Lucas, P. W., Roche, P. F., Allard, F., & Hauschildt, P. H. 2001, *MNRAS*, 326, 695
- Luhman, K. L. 1999, *ApJ*, 525, 466
- Luhman, K. L. 2024, *AJ*, 168, 230
- Luhman, K. L. 2025, *AJ*, in press
- Luhman, K. L., Alves de Oliveira, C., Baraffe, I., et al. 2024, *AJ*, 167, 19
- Luhman, K. L., Esplin, T. E., & Loutrel, N. P. 2016, *ApJ*, 827, 52
- Luhman, K. L., & Hapich, C. J. 2020, *AJ*, 160, 57
- Luhman, K. L., Lada, E. A., Hartmann, L., et al. 2005a, *ApJ*, 631, L69
- Luhman, K. L., Lada, E. A., Muench, A. A., & Elston, R. J. 2005a, *ApJ*, 618, 810
- Luhman, K. L., Liebert, J., & Rieke, G. H. 1997, *ApJL*, 489, L165
- Luhman, K. L., Mamajek, E. E., Shukla, S. J., & Loutrel, N. P. 2017, *AJ*, 153, 46
- Luhman, K. L., McLeod, K. K., & Goldenson, N. 2005c, *ApJ*, 623, 1141
- Luhman, K. L., Rieke, G. H., Lada, C. J., & Lada, E. A. 1998, *ApJ*, 508, 347
- Luhman, K. L., Stauffer, J. R., Muench, A. A., et al. 2003, *ApJ*, 593, 1093
- Luhman, K. L., Tremblin, P., Birkmann, S. M., et al. 2023, *ApJL*, 949, L36
- Martín, E. L., Basri, G., Delfosse, X., & Forveille, T. 1997, *A&A*, 327, L29
- Matrajt, G., Muñoz Caro, G. M., Dartois, E., et al. 2005, *A&A*, 433, 979
- Meyer, M. R., Flaherty, K., Levine, J. L., et al. 2008, in *Handbook of Star Forming Regions*, Vol. 1, ed. B. Reipurth (San Francisco, CA: ASP), 662
- Muench, A. A., Lada, C. J., Luhman, K. L., Muzerolle, J., & Young, E. 2007, *AJ*, 134, 411
- Nakajima, T., Oppenheimer, B. R., Kulkarni, S. R., et al. 1995, *Nature*, 378, 463
- Opitz, D., Tinney, C. G., Faherty, J., et al. 2016, *ApJ*, 819, 17
- Oppenheimer, B. R., Kulkarni, S. R., Nakajima, T., & Matthews, K. 1995, *Science*, 270, 1478
- Pendleton, Y. J., & Allamandola, L. J. 2002, *ApJS*, 138, 75
- Pendleton, Y. J., Sandford, S. A., Allamandola, L. J., Tielens, A. G. G. M., & Sellgren, K. 1994, *ApJ*, 437, 683
- Petrus, S., Chauvin, G., Bonnefoy, M., et al. 2023, *A&A*, 670, L9
- Rebolo, R., Martín, E. L., Basri, G., et al. 1996, *ApJ*, 469, L53
- Rebolo, R., Zapatero Osorio, M. R., & Martín, E. L. 1995, *Nature*, 377, 129
- Rieke, M. J., Kelly, D. M., & Horner, S. 2005, *SPIE*, 5904, 590401
- Rieke, M. J., Kelly, D. M., Misselt, K., et al. 2023, *PASP*, 135, 028001
- Robberto, M., Gennaro, M., Da Rio, N., et al. 2024, *ApJ*, 960, 49
- Robin, A. C., Reylé, C. Derrière, S., & Picaud, S. 2003, *A&A*, 409, 523
- Sandford, S. A., Allamandola, L. J., Tielens, A. G. G. M., et al. 1991, *ApJ*, 371, 607
- Schlafly, E. F., Meisner, A. M., Stutz, A. M., et al. 2016, *ApJ*, 821, 78
- Seo, H. H., & Scholz, A. 2025, *MNRAS*, 537, 2579
- Soifer, B. T., Russell, R. W., & Merrill, K. M. 1976, *ApJL*, 207, L83
- Stauffer, J. R., Hamilton, D., & Probst, R. G. 1994, *AJ*, 108, 155
- Tinney, C. G., Burgasser, A. J., & Kirkpatrick, J. D. 2003, *AJ*, 126, 975
- Todorov, K., Luhman, K. L., & McLeod, K. K. 2010, *ApJL*, 714, L84
- Todorov, K., Luhman, K. L., Konopacky, Q. M., et al. 2014, *ApJ*, 788, 40
- Tremblin, P., Amundsen, D. S., Mourier, P., et al. 2015, *ApJL*, 804, L17
- Tremblin, P., Chabrier, G., Baraffe, I., et al. 2017, *ApJ*, 850, 46
- Vrba, F. J., Henden, A. A., Luginbuhl, C. B., et al. 2004, *AJ*, 127, 2948
- Wdowiak, T. J., Flickinger, G. C., & Cronin, J. R. 1988, *ApJL*, 328, L75
- Zhang, Z., Molliére, P., Fortney, J., & Marley, M. S. 2025, *AJ*, submitted

Table 1. NIRCcam Data for Previously Known and Candidate Members of IC 348

Column Label	Description
LRL	LRL source name ^a
RAdeg	Right ascension (ICRS)
DEdeg	Declination (ICRS)
m162mag	F162M NIRCcam magnitude
e_m162mag	Error in m162mag
m182mag	F182M NIRCcam magnitude
e_m182mag	Error in m182mag
m360mag	F360M NIRCcam magnitude
e_m360mag	Error in m360mag
m444mag	F444W NIRCcam magnitude
e_m444mag	Error in m444mag
memberstatus	Previously known member or candidate member

^a Source names are a continuation of the designation numbers from [Luhman et al. \(1998\)](#). Sources 1, 3, and 4 from L24 are assigned LRL numbers of 11001, 11003, and 11004, respectively.

NOTE— The table is available in its entirety in machine-readable form.

Table 2. Sources in IC 348 Observed with NIRSpect

LRL ^a	α (ICRS)	δ (ICRS)	Membership Status	Spectral Classification	Log L/L_{\odot}
Brown Dwarf Candidates					
2121	56.044617	32.234873	new member	H	-3.51 ± 0.17
2296	56.021553	32.235174	new member	H	-3.29 ± 0.16
11024	55.995656	32.040611	new member	H	-4.77 ± 0.12
11027	55.980488	32.031945	new member	M9–L2	-3.52 ± 0.12
11037	56.101440	32.241459	new member	H	-4.88 ± 0.12
11040	56.280767	32.257480	new member	H	-4.98 ± 0.12
11041	56.259664	32.238901	new member	H	-4.95 ± 0.11
11043	56.224701	32.230297	new member	H	-3.88 ± 0.13
11044	56.224665	32.230241	new member	H	-3.17 ± 0.14
11032	56.063180	32.215357	background	T2	...
11042	56.242072	32.262070	background	T2	...
11046	56.000765	32.165685	background	mid-T	...
11049	56.005416	32.115411	background	T4	...
11047	56.002391	32.105789	background	galaxy ($z=3.31$)	...
11048	55.985803	32.152554	background	galaxy ($z=1.30$)	...
Filler Targets					
1546	56.030318	32.242502	previous member	M9–L1	-2.78 ± 0.14
22705	56.286963	32.262969	previous member	M9–L1	-2.90 ± 0.13
40013	56.092171	32.236212	previous member	H	-3.09 ± 0.12
11039	56.093226	32.244790	background	galaxy ($z=3.54$)	...
11023	55.993680	32.046580	background	highly reddened star	...
11025	55.990609	32.036538	background	highly reddened star	...
11030	56.016966	32.028483	background	highly reddened star	...
11031	56.021736	32.016230	background	highly reddened star	...

^a Source names are a continuation of the designation numbers from Luhman et al. (1998).

Table 3. NIRCcam Data for Candidate Members ($\geq L0$) of NGC 2024

ID	α (ICRS)	δ (ICRS)	m_{115}	m_{140}	m_{182}	m_{360}	m_{444}
			(mag)	(mag)	(mag)	(mag)	(mag)
1	85.406934	-1.869930	20.31±0.02	18.66±0.02	16.96±0.02	15.43±0.02	15.12±0.02
2	85.412144	-1.883558	...	24.75±0.08	21.98±0.03	19.56±0.11	19.21±0.12
3	85.415234	-1.923661	20.87±0.02	17.96±0.05	17.54±0.04
4	85.415437	-1.896986	22.20±0.03	18.72±0.07	18.16±0.05
5	85.416883	-1.949274	21.82±0.02	18.99±0.06	18.54±0.04
6	85.430595	-1.940618	22.22±0.02	21.11±0.02	19.59±0.02	18.01±0.02	17.61±0.02
7	85.431232	-1.867624	25.35±0.04	24.08±0.03	22.05±0.02	19.77±0.06	19.21±0.03
8	85.439093	-1.928280	22.87±0.02	21.84±0.02	19.72±0.02	16.38±0.02	15.83±0.02

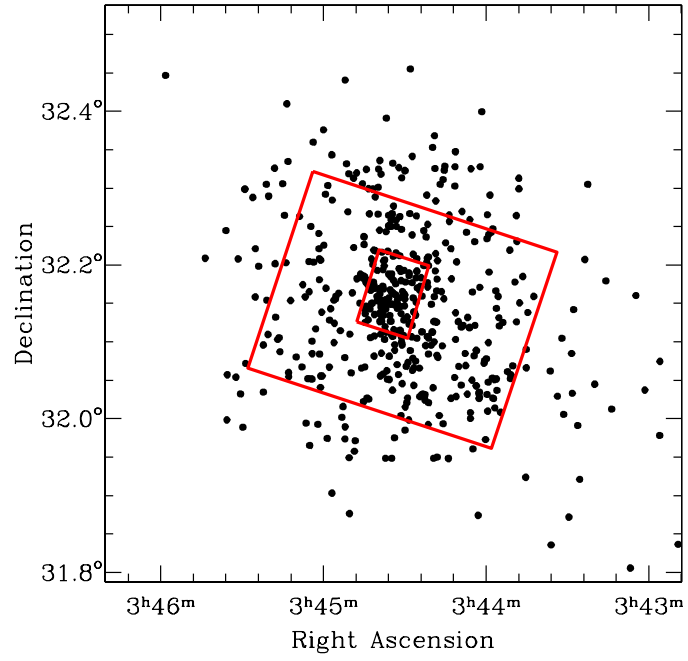


Figure 1. Map of the known members of IC 348 prior to this work and the fields imaged by JWST/NIRCam in Cycles 1 and 3 (inner and outer rectangles).



Figure 2. JWST/NIRCam images in three filters (F162M, F360M, F444W) from Cycle 3 for a $16' \times 20'$ field in IC 348.

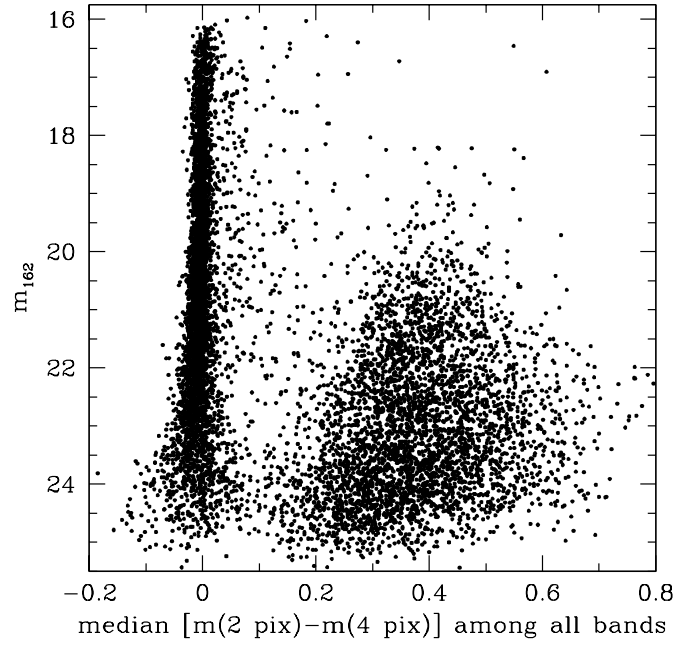


Figure 3. m_{162} versus the median difference between 2 and 4 pixel aperture photometry among the available bands for sources in NIRCcam images of IC 348 from Cycle 3. This metric is used to classify the sources as point-like (< 0.1) or extended (≥ 0.1).

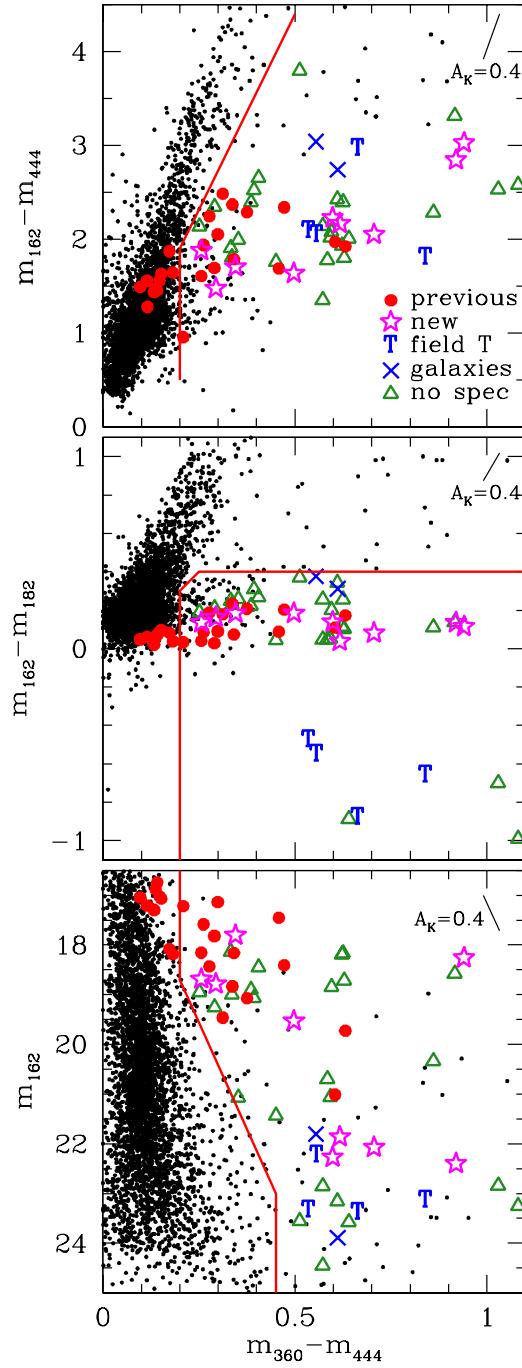


Figure 4. Color-color and color-magnitude diagrams for point sources in NIRCcam images of IC 348 from Cycle 3. We have marked the previously known members that are not saturated and the candidate members identified with these diagrams, some of which have been classified as new members, field T dwarfs, or galaxies with NIRSpc (Table 2). The criteria used for selecting candidates are indicated (solid lines).

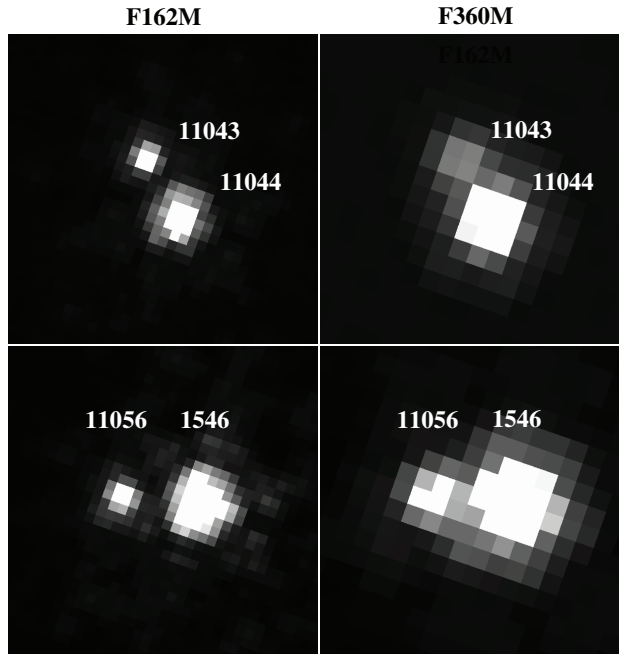


Figure 5. JWST/NIRCam images of two close pairs in IC 348. LRL 1546 is a previously known brown dwarf while LRL 11043 and LRL 11044 are classified as new brown dwarfs with NIRSpec (Figure 7). LRL 11056 lacks spectroscopy, but its colors are consistent with a late spectral type. The size of each image is $1'' \times 1''$. North is up and east is left.

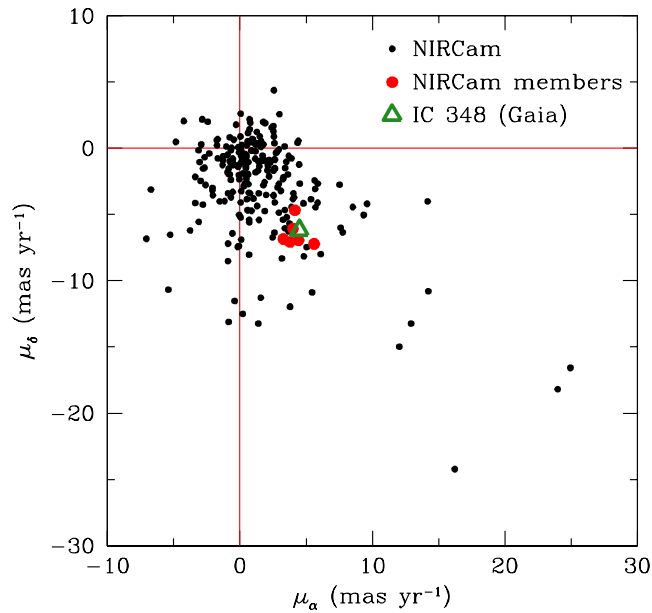


Figure 6. Proper motions measured for point sources in JWST/NIRCam images of IC 348 from Cycles 1 and 3. We have marked the six previously known members of the cluster that appear in both epochs and are not saturated, three of which were discovered with the Cycle 1 data. We also indicate the proper motion of the cluster based on Gaia DR3.

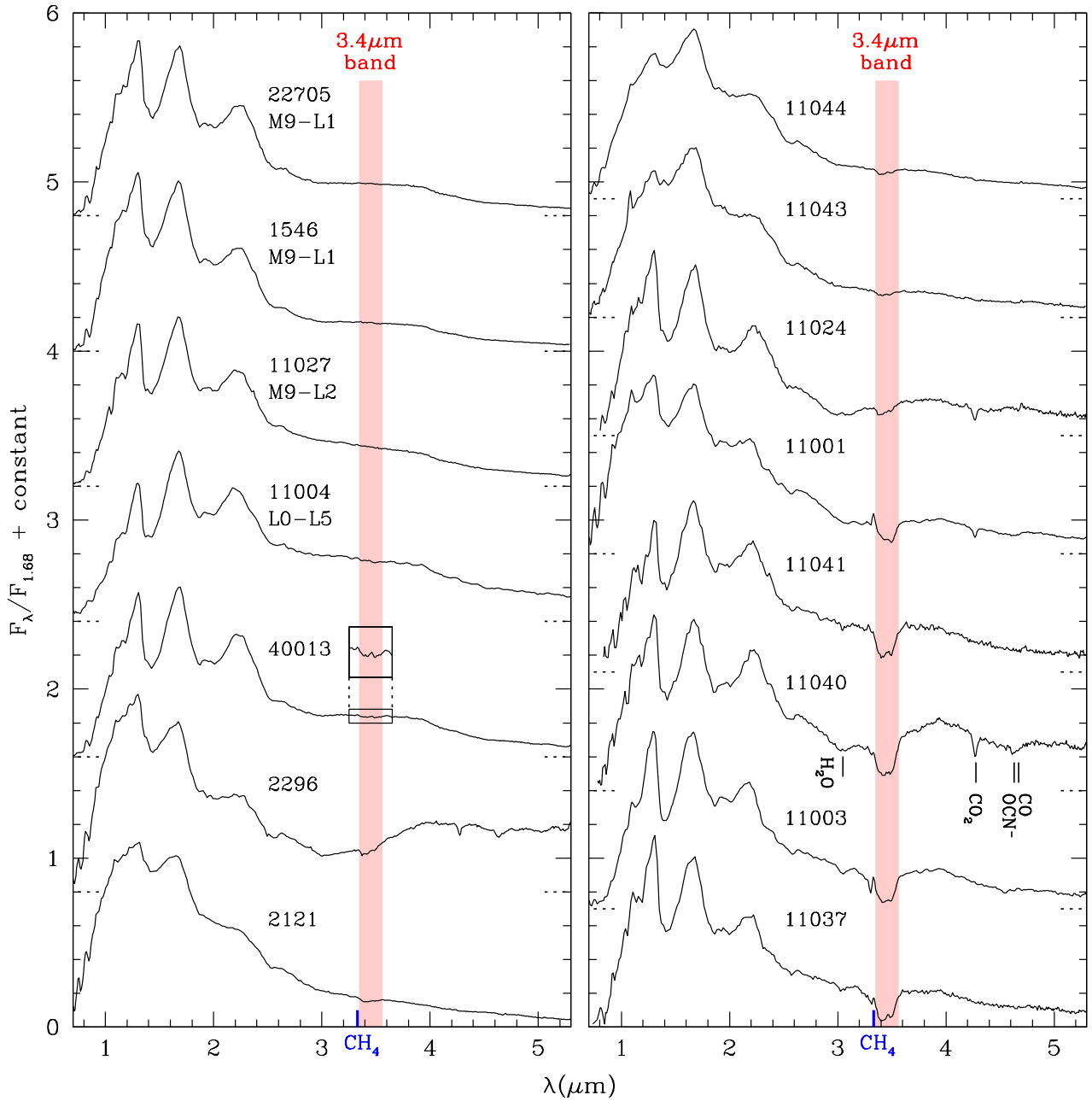


Figure 7. JWST/NIRSpec spectra collected in this work and in L24 for brown dwarfs in IC 348. The first four objects are normal young L dwarfs. The remaining sources exhibit the $3.4 \mu\text{m}$ feature from an unidentified aliphatic hydrocarbon. The wavelength range of that feature is marked by the pink band. For reference, the central wavelength of the Q branch of CH_4 (not detected in these objects) is indicated by the blue tick mark. Two brown dwarfs (LRL 2296, LRL 11040) have large excess emission at $>3.5 \mu\text{m}$ and absorption features that may arise from ices (H_2O , CO_2 , OCN^- , CO). For each spectrum that has been shifted upward, the level for zero flux is marked by a pair of dotted tick marks.

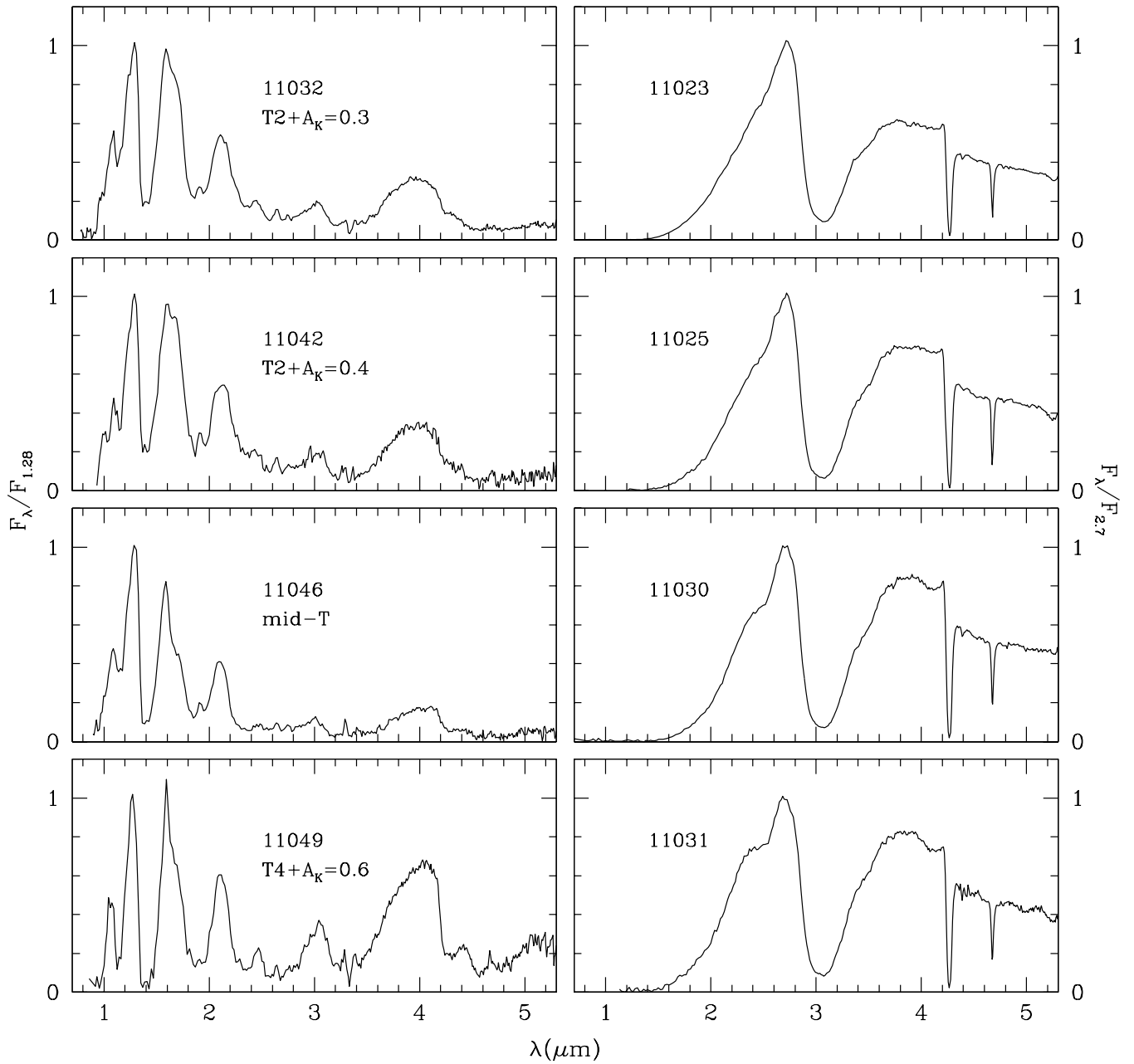


Figure 8. JWST/NIRSpec spectra for brown dwarf candidates in IC 348 that are background T dwarfs (left) and highly reddened background stars that were selected as filler targets (right).

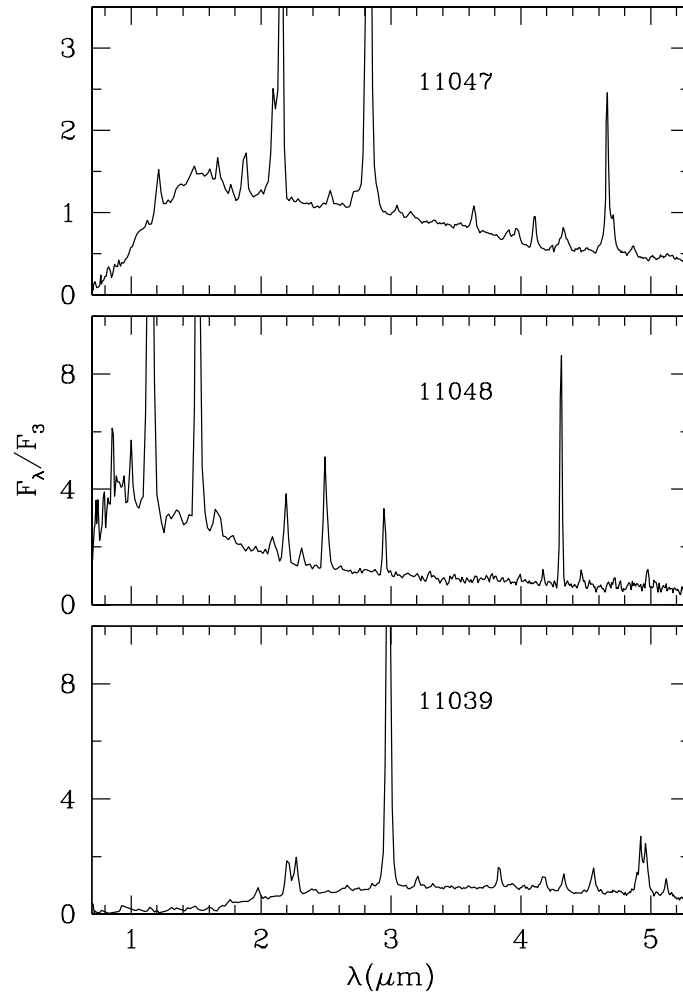


Figure 9. JWST/NIRSpec spectra for two brown dwarf candidates in IC 348 and a filler target that are active galaxies.

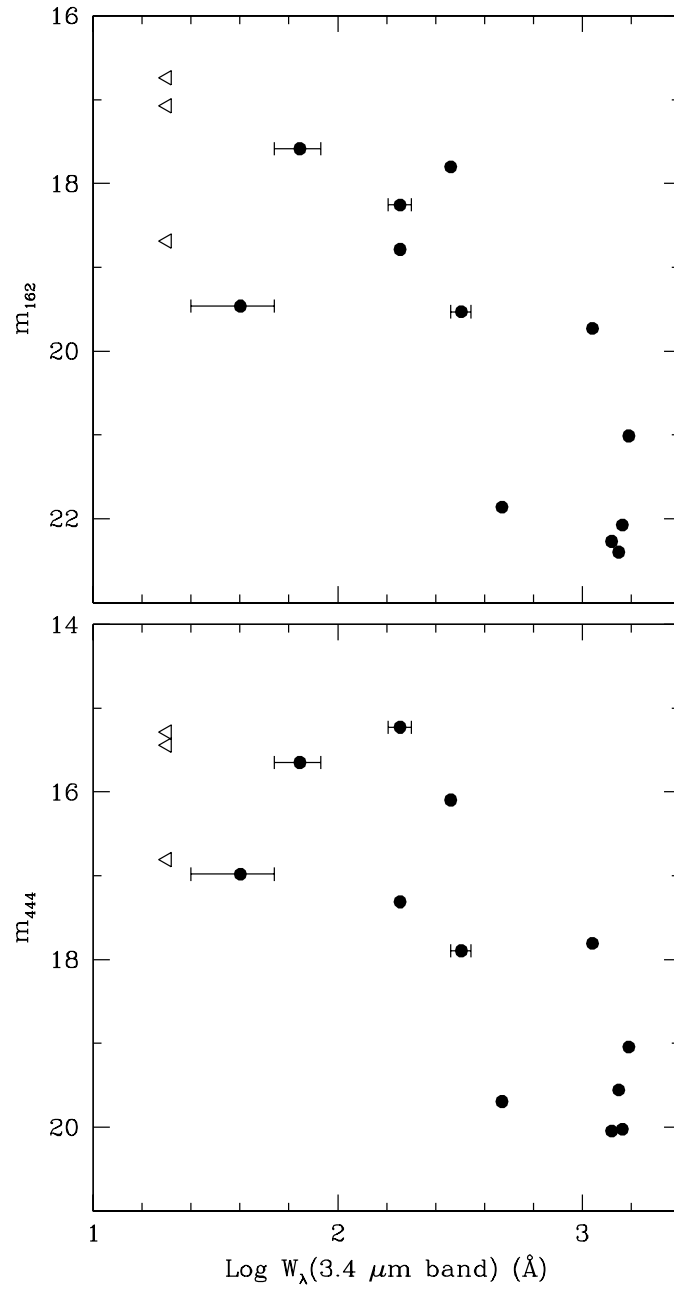


Figure 10. Photometry in F162M and F444W versus the equivalent width of the $3.4 \mu\text{m}$ feature for brown dwarfs in IC 348 (Figure 7). Error bars are omitted when they are smaller than the symbols.

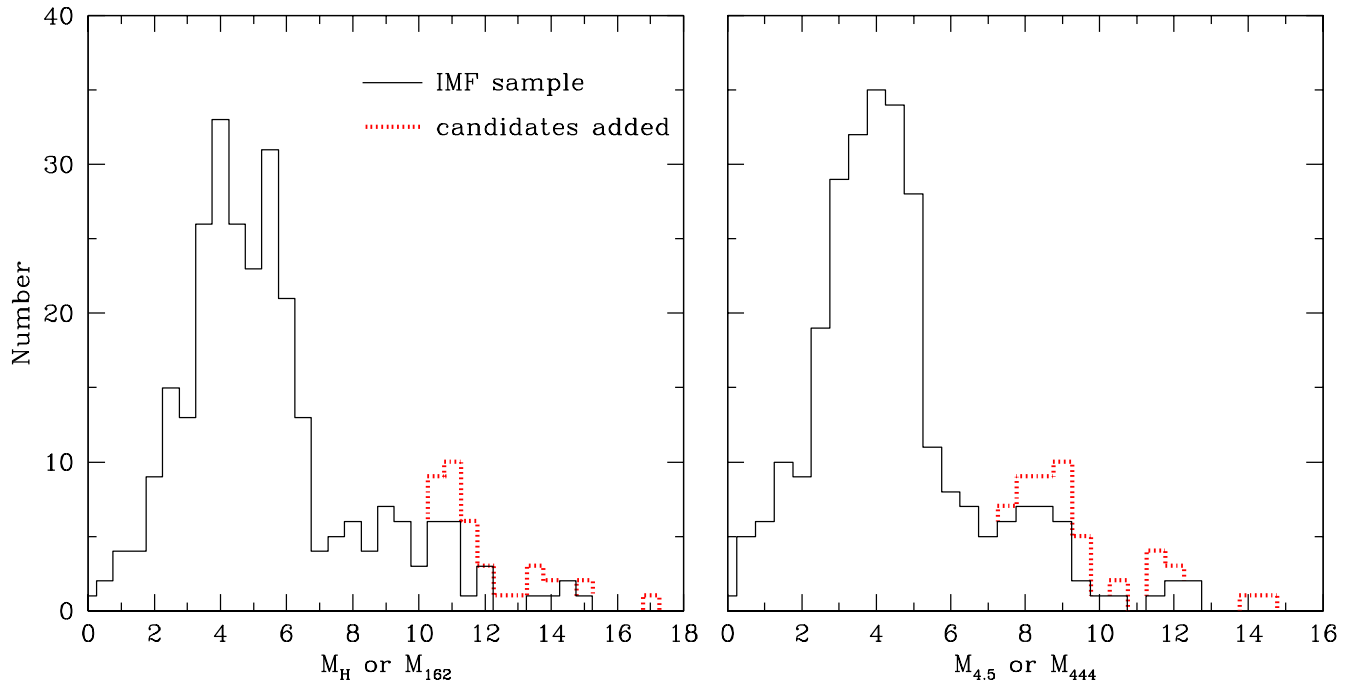


Figure 11. Histograms of extinction-corrected absolute magnitudes in H or F162M (left) and $[4.5]$ or F444W (right) for known members of IC 348 in our IMF sample (solid line) and the remaining viable NIRCcam candidates that lack spectroscopy (dotted line).

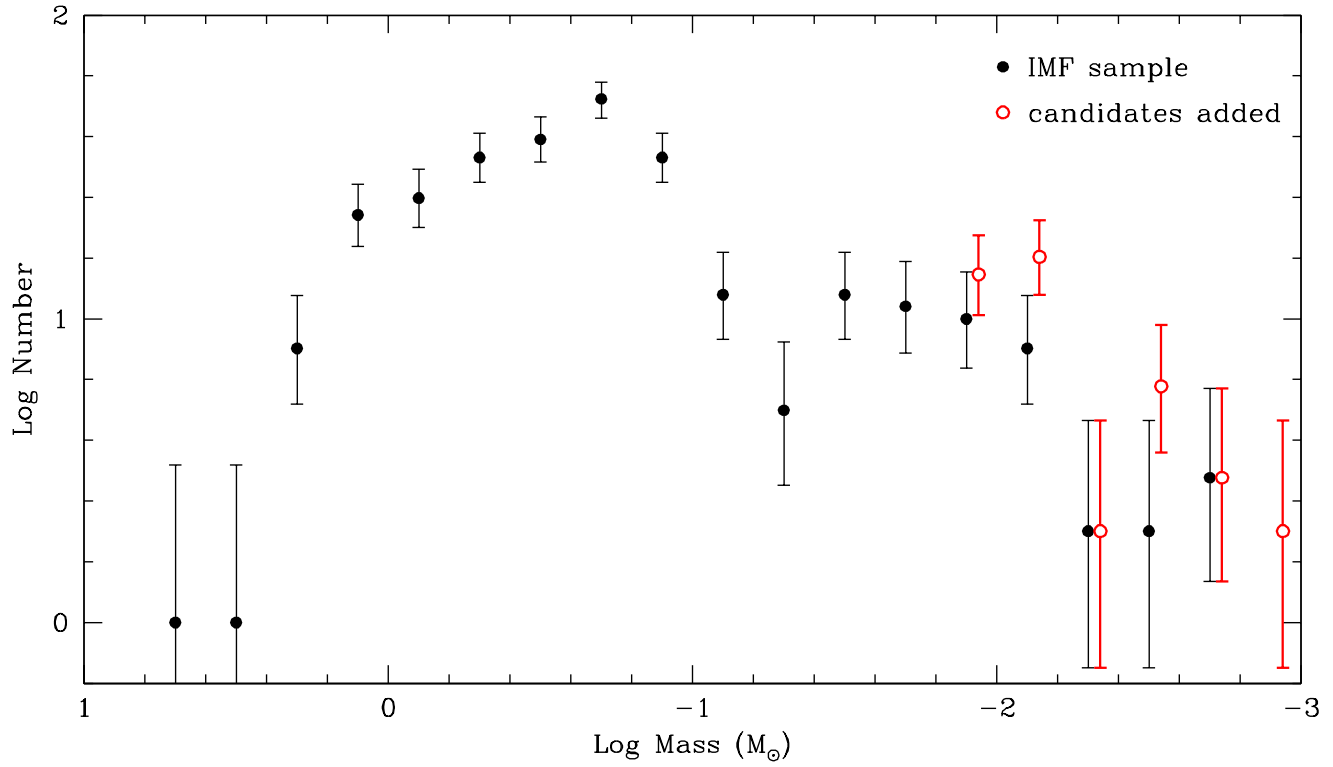


Figure 12. IMF for an extinction-limited sample of members of IC 348 within the NIRCcam field (points) and the mass function after including the remaining viable candidates from NIRCcam that lack spectroscopy (open circles). The latter points are shifted slightly in mass for clarity.

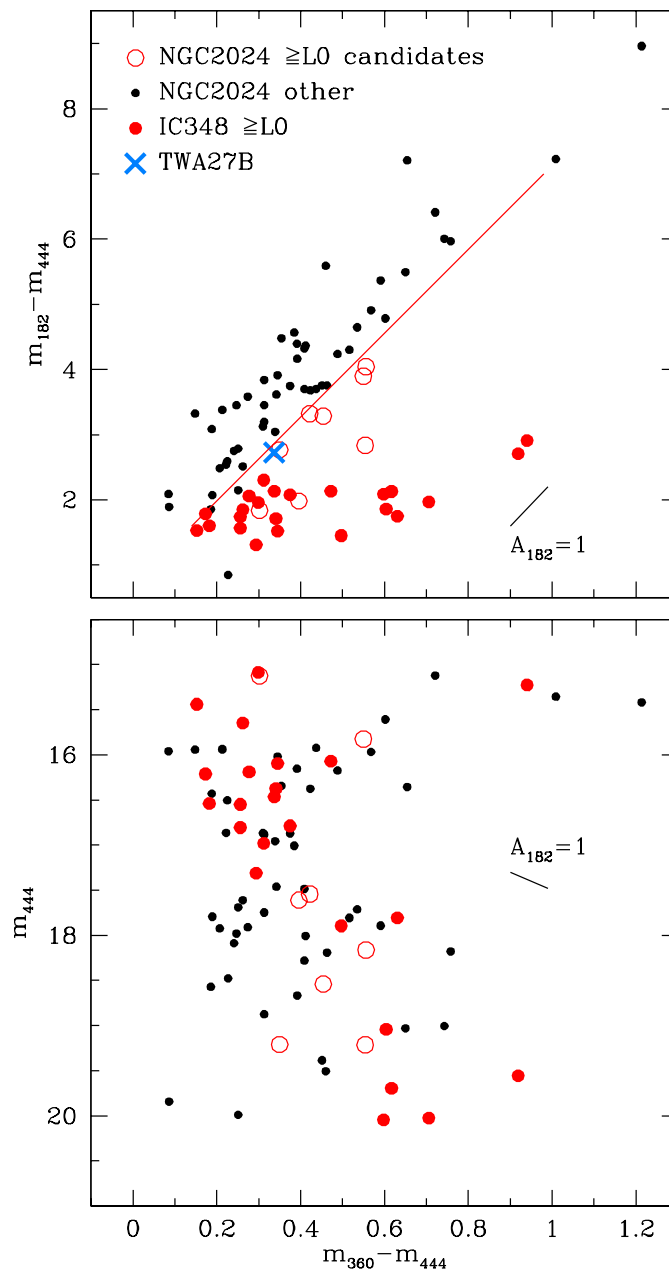


Figure 13. Color-color and color-magnitude diagrams for sources in JWST/NIRCam images of NGC 2024 (black points and red circles), members of IC 348 with types of $\geq L0$ (red points), and TWA 27B (cross). The latter is shown in only the top diagram. The red line is a reddening vector used for selecting the $\geq L0$ candidates in NGC 2024.